nature plants

SUPPLEMENTARY INFORMATION

https://doi.org/10.1038/s41477-020-0632-4

In the format provided by the authors and unedited.

# Real-time detection of wound-induced $H_2O_2$ signalling waves in plants with optical nanosensors

**Tedrick Thomas Salim Lew[1,2], Volodymyr B. Koman[1], Kevin S. Silmore[1], Jun Sung Seo[2,3], Pavlo Gordiichuk[1], Seon-Yeong Kwak[4], Minkyung Park[1,2], Mervin Chun-Yi Ang[2], Duc Thinh Khong[2,5], Michael A. Lee[1], Mary B. Chan-Park[2,5], Nam-Hai Chua[2,3] and Michael S. Strano[1,2] ✉**

[1]Department of Chemical Engineering, Massachusetts Institute of Technology, Cambridge, MA, USA. [2]Disruptive & Sustainable Technologies for Agricultural Precision IRG, Singapore-MIT Alliance for Research and Technology, 1 CREATE Way, #03-06/07/08 Research Wing, Singapore, Singapore. [3]Temasek Life Sciences Laboratory Limited, 1 Research Link National University of Singapore, Singapore, Singapore. [4]Department of Biosystems and Biomaterials Science and Engineering, Seoul National University, Seoul, Republic of Korea. [5]School of Chemical and Biomedical Engineering, Nanyang Technological University, Singapore, Singapore. ✉e-mail: strano@mit.edu

# Supplementary Information

## Real-time Detection of Wound-Induced $H_2O_2$ Signalling Waves in Plants with Optical Nanosensors

Tedrick Thomas Salim Lew[1,2], Volodymyr B. Koman[1], Kevin S. Silmore[1], Jun Sung Seo[2,3], Pavlo Gordiichuk[1], Seon-Yeong Kwak[4], Minkyung Park[1,2], Mervin Chun-Yi Ang[2], Khong Duc Thinh[2], Michael A. Lee[1], Mary B. Chan-Park[2,5], Nam-Hai Chua[2,3] and Michael S. Strano[1,2,*]

[1]Department of Chemical Engineering, Massachusetts Institute of Technology, 77 Massachusetts Avenue, Cambridge, MA 02139, USA
[2]Disruptive & Sustainable Technologies for Agricultural Precision IRG, Singapore-MIT Alliance for Research and Technology, 1 CREATE Way, #03-06/07/08 Research Wing, Singapore 138602, Singapore
[3]Temasek Life Sciences Laboratory Limited, 1 Research Link National University of Singapore, Singapore 117604, Singapore
[4]Department of Biosystems and Biomaterials Science and Engineering, Seoul National University, Seoul 151-921, Republic of Korea
[5]School of Chemical and Biomedical Engineering, Nanyang Technological University, 62, Nanyang Drive, Singapore 637 459, Singapore

*Corresponding author's email address: strano@mit.edu

## Supplementary Discussion

### Reversible First-Order Binding Model

The binding event between G-SWNT and $H_2O_2$ can be described as a first-order reversible reaction:

$$S + A \underset{k_b}{\overset{k_f}{\rightleftarrows}} S\text{-}A \quad (1)$$

where S and A represents G-SWNT and $H_2O_2$ respectively, S-A is the binding complex formed between G-SWNT and $H_2O_2$, and $k_f$ and $k_b$ are the forward and backward rate constants. The rate of reaction can be described by the following differential equation:

$$\frac{d[S]}{dt} = -k_f[S][A] + k_b[S-A] \quad (2)$$

At the initial stage of binding interaction, the G-SWNT and analyte concentrations are close to their original concentrations, i.e. $[S] \approx [S]_0$ and $[A] \approx [A]_0$. The reaction can therefore be assumed to be almost completely forward, and the above equation can be simplified to

$$\left.\frac{d[S]}{dt}\right|_{t\to 0} = -k_f[S]_0[A]_0 \quad (3)$$

By assuming that the normalized sensor response ($\frac{I}{I_0}$) is proportional to the normalized sensor concentration, i.e. $\frac{I}{I_0} = \frac{[S]}{[S]_0}$ , we can estimate $k_f$ from the initial change of the sensor intensity upon the addition of $H_2O_2$ in vitro:

$$k_f = \frac{1}{[A]_0} \frac{d\frac{[I]}{[I]_0}}{dt}\Bigg|_{t\to 0} \tag{4}$$

At equilibrium, the forward and backward reaction rates are equal and we can obtain $k_b$:

$$k_b = k_f \frac{\frac{[I]}{[I]_0}[A]}{1-\frac{[I]}{[I]_0}} \tag{5}$$

From the above expressions, we obtained $k_f$ and $k_b$ to be approximately 147 $M^{-1}$ $s^{-1}$ and 0.0131 $s^{-1}$ respectively. The approximate $H_2O_2$ concentration can be obtained from the in vivo sensor intensity profile after extracting the estimates of $k_f$ and $k_b$ from in vitro experiments:

$$[A] = \frac{k_b\left(1-\frac{[I]}{[I]_0}\right) - \frac{d\frac{[I]}{[I]_0}}{dt}}{k_f \frac{[I]}{[I]_0}} \tag{6}$$

**Simulation Model of $H_2O_2$ Wave Propagation:**

We consider an autocatalytic $H_2O_2$ (A) production from a static precursor species (P) which does not diffuse, and a first-order decay reaction of A:

$$A + P \xrightarrow{k_p} A + A \tag{7}$$

$$A \xrightarrow{k_d} B \tag{8}$$

The mass balances of A and P in one-dimensional system are as follows:

$$\frac{\partial A}{\partial t} = D\frac{\partial^2 A}{\partial z^2} + k_P PA - k_d A \tag{9}$$

$$\frac{\partial P}{\partial t} = -k_P PA \tag{10}$$

To facilitate mathematical solution, we can introduce non-dimensional variables:

$$x = \frac{z}{\delta};\quad \delta = \sqrt{\frac{D}{k_P P_0}} \tag{11}$$

$$\overline{P} = \frac{P}{P_0};\quad \overline{A} = \frac{A}{P_0} \tag{12}$$

$$\tau = \frac{t}{t_c} = \frac{Dt}{\delta^2} \tag{13}$$

$$\alpha = \frac{k_d}{k_P} \tag{14}$$

The non-dimensional mass balances and initial conditions are therefore as follows:

$$\frac{\partial \overline{A}}{\partial \tau} = \frac{\partial^2 \overline{A}}{\partial x^2} + \overline{P}\,\overline{A} - \alpha \overline{A} \tag{15}$$

$$\frac{\partial \overline{P}}{\partial \tau} = -\overline{P}\,\overline{A} \tag{16}$$

Here, $\alpha$ is the ratio between the consumption and production rate of $H_2O_2$, and can therefore be considered as a proxy for the innate antioxidant level within each plant species. In this work, we define $\alpha$ as the $H_2O_2$ decay rate. A simple linear stability analysis can be conducted by introducing a perturbation in A and P of the form $\boldsymbol{\varepsilon} e^{\sigma t - i\mathbf{k}\cdot\mathbf{x}}$ around the fixed point of (A*, P*) = (0,1), which yields the following eigenvalue equation:

$$\sigma \boldsymbol{\varepsilon} = \begin{bmatrix} -k^2 + (1-\alpha) & 0 \\ -1 & 0 \end{bmatrix} \boldsymbol{\varepsilon} \tag{17}$$

Wavevectors that satisfy $k^2 < 1 - \alpha$ are unstable. Given that traveling waves are observed, this indicates that small concentrations of A can result in large waves when $\alpha < 1$, and the traveling waves will be extinguished when $\alpha > 1$.

The governing equations were numerically solved via the method of lines, where the spatial derivatives were approximated via the finite volume method. Integration in time was performed with the adaptive stiff ODE solver, *ode15s*, in MATLAB. The width of the finite volume cells was 0.004. The initial concentration of A was set to a nonzero but constant value in a small region near the left boundary and allowed to develop into a traveling wave. This small step-like disturbance was chosen to mimic a wounding event. For sharp initial disturbances, we have found that the speed of the resultant wave is the smallest possible one that the model allows. The left boundary condition for A is in an insulating (Neumann) boundary condition, and the right boundary condition for A is fixed at 0 (Dirichlet), though the domain is set to be large enough for each value of $\alpha$ such that the wave never touches the right boundary and the concentration of A near the right boundary remains negligible.

From the simulation, the wave speed can be obtained by measuring the time taken for the level of A at a particular distance from the source to reach half of its amplitude. Given a sharp initial disturbance of A, the wave speed is uniquely determined by $\alpha$ and does not depend on the simulation time, distance or the initial disturbance amplitude. As $\alpha$ increases, the first-order decay reaction becomes more significant and the wave speed decreases (Figure 5d). It can be shown that the traveling wave velocity, *c*, depends on $\alpha$ as follows:

$$c^2 = c_{\alpha=0}^2(1-\alpha) \tag{18}$$

where $c_{\alpha=0}$ is the wave velocity when $\alpha = 0$. This model thus supports the idea that the different capacity of plants to produce and scavenge $H_2O_2$ contributes to the heterogeneity in apparent wave speed observed across species.

For comparison with experimentally-measured wave speed, the propagating wave generated from numerical simulation was fitted to the temporal profile of wound-induced $H_2O_2$ concentration change measured experimentally (from the optical sensor response) for each plant species. This yields the best-fit $\alpha$ for a particular plant species, which corresponds to a specific wave speed obtained from the numerical simulation. The fitting also yields scaling parameters for concentration (y-axis) and time (x-axis). The wave speed was then converted into dimensional form, using scaling parameters for concentration and time, for comparison with experimentally-measured wave speed.

## Supplementary Figures

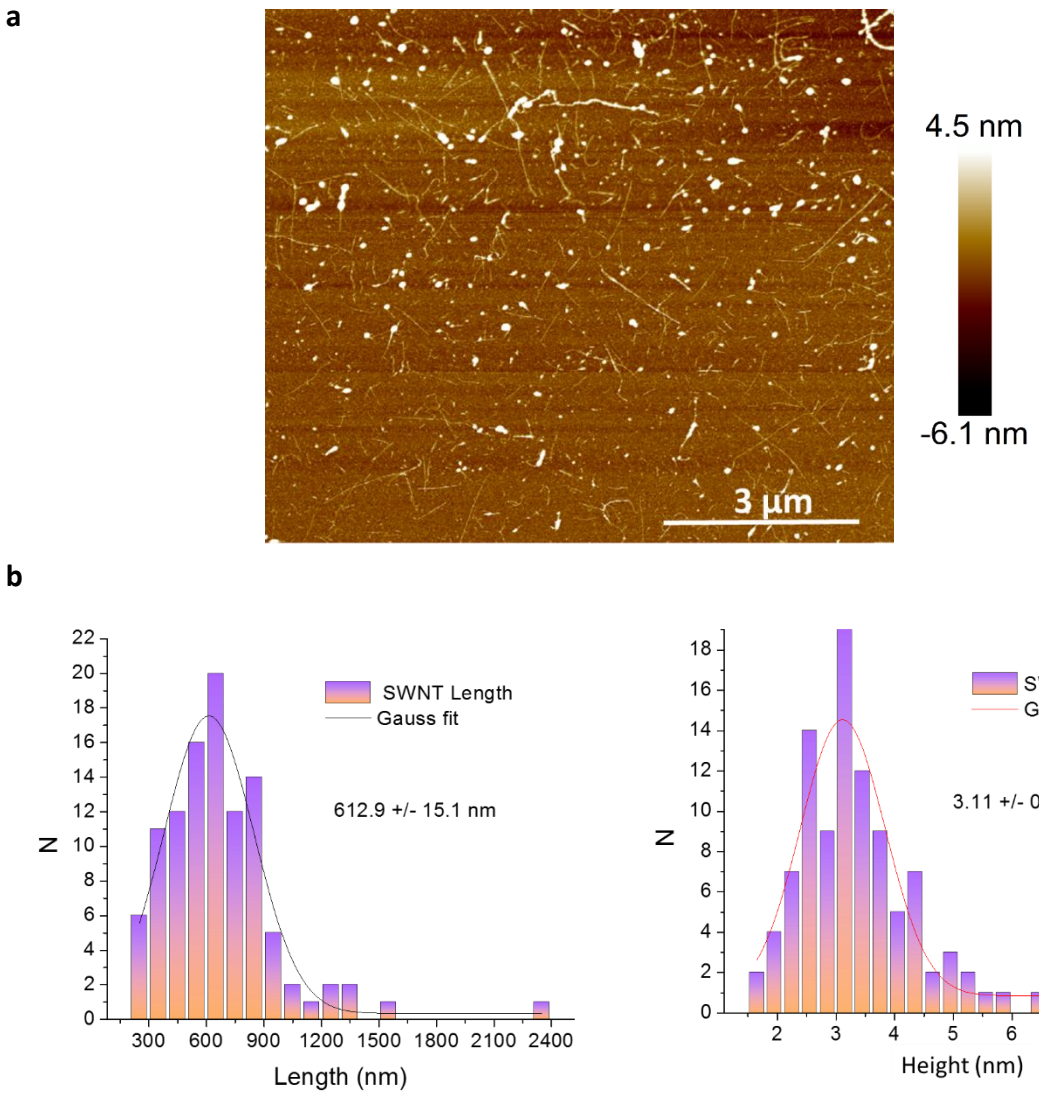


**Supplementary Figure 1. High resolution microscopy of G-SWNT. a,** AFM image of G-SWNT on mica surface. **b**, Length and height profiles of individual G-SWNT analyze through AFM images.

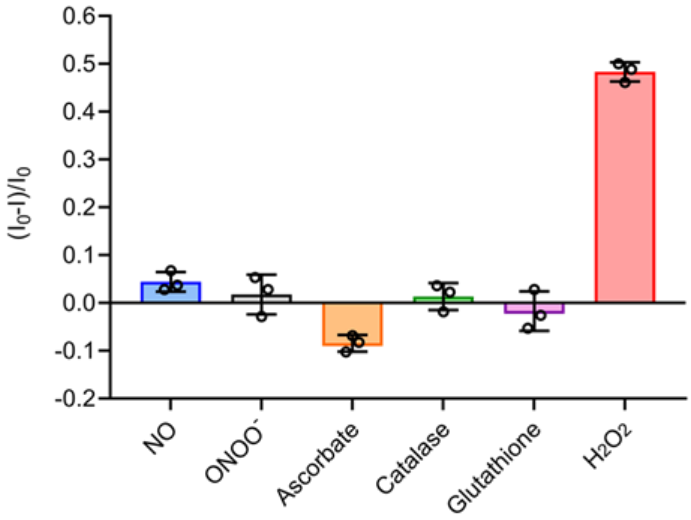


**Supplementary Figure 2. G-SWNT sensor response towards other radical reactive species and $H_2O_2$ scavengers commonly present in a plant cell.** No significant sensor response towards these analytes was detected as compared to the sensor response towards $H_2O_2$. Data are mean ± s.d. from three independent experiments.

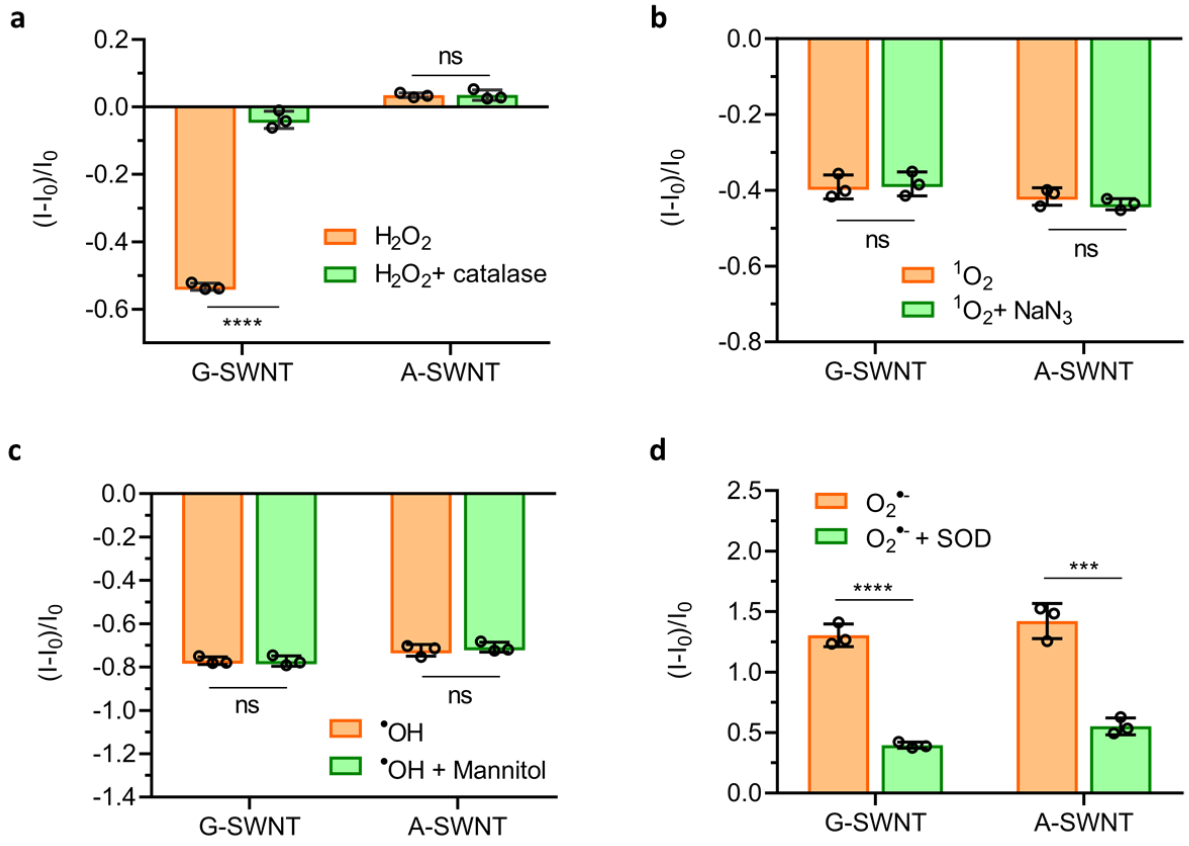


**Supplementary Figure 3. Fluorescence intensity modulation of G-SWNT and A-SWNT in response to ROS and their scavengers. a,** $H_2O_2$ results in a reversible quenching of G-SWNT, while A-SWNT intensity remains invariant. Data are mean ± s.d. from three independent experiments. Two-tailed unpaired t-test, ****P < 0.0001, P = 0.977 for A-SWNT. ns = not statistically significant. **b,** $^1O_2$ and **c,** ·OH result in irreversible decrease of both G-SWNT and A-SWNT with similar magnitude. Data are mean ± s.d. from three independent experiments. Two-tailed unpaired t-test, P = 0.776 and P = 0.265 for G-SWNT and A-SWNT respectively in $^1O_2$ test, P = 0.922 and P = 0.510 for G-SWNT and A-SWNT respectively in ·OH test. ns = not statistically significant. **d,** $O_2{\cdot}^-$ gives rise to a reversible increase of fluorescence intensity of both G-SWNT and A-SWNT with similar magnitude. Data are mean ± s.d. from three independent experiments. Two-tailed unpaired t-test, ****P < 0.0001 and ***P < 0.001. The analyte concentration is 100 μM in all experiments.

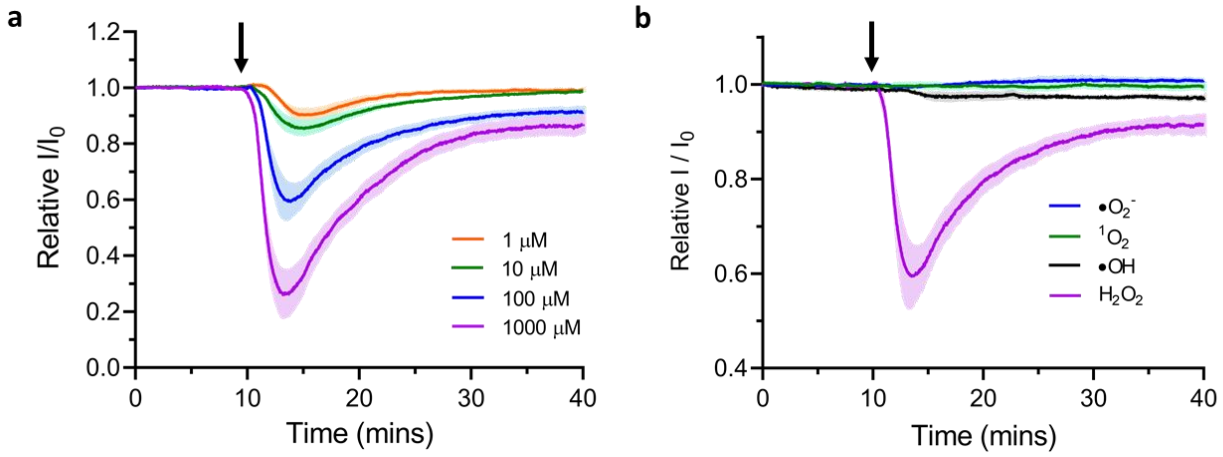


**Supplementary Figure 4. In vivo sensor response towards ROS infiltration on a spinach leaf.** **a,** Dose responses exhibited by the relative intensity profile of G-SWNT to A-SWNT upon the infiltration of varying concentrations of $H_2O_2$. Relative intensity profile was obtained by taking the ratio between G-SWNT and A-SWNT fluorescence intensity at each time point, normalized with their initial values. **b,** The ratiometric sensor profile upon the infiltration of 100 μM $H_2O_2$, $^1O_2$, ·OH and $O_2^{\cdot -}$ onto the leaf. Black arrow indicates the time point of analyte infiltration. Shaded regions represent s.e.m. from $n$ = 5 biologically independent plants.

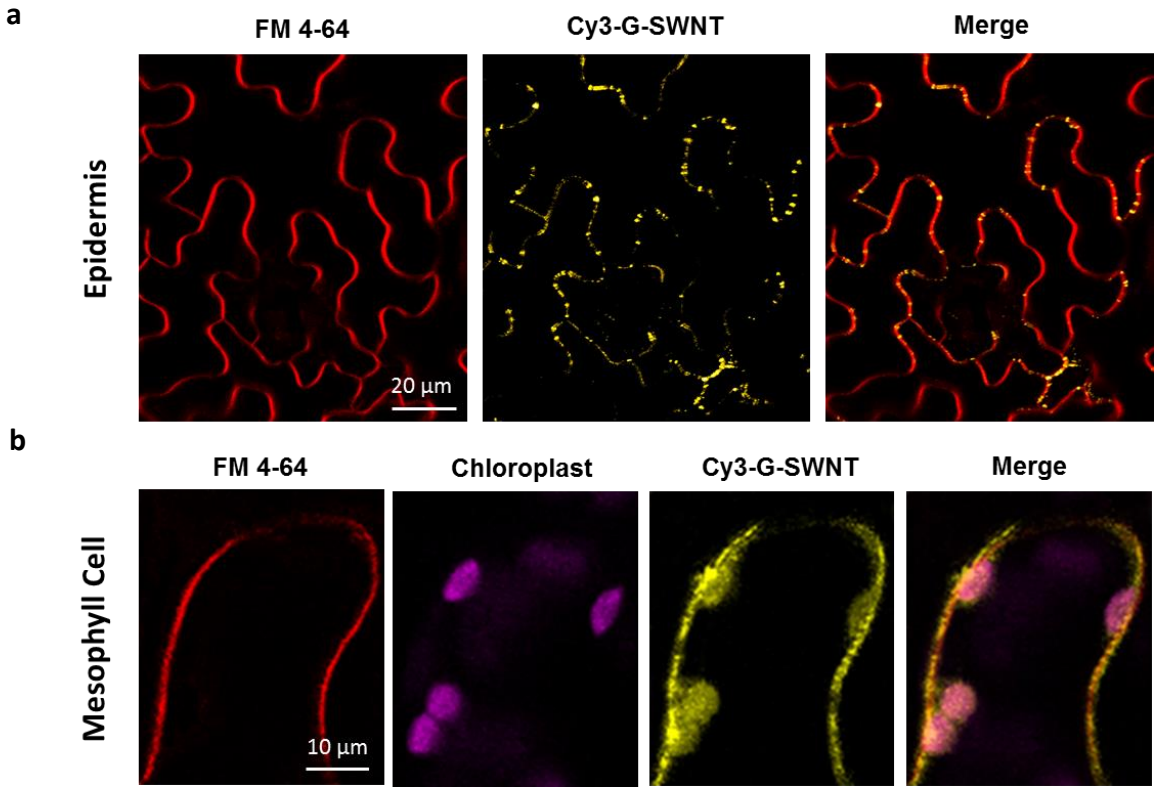


**Supplementary Figure 5. Localization of dye-labelled G-SWNT in spinach plant leaf tissue.** **a,** Fluorescence confocal micrographs of Cy3-labelled G-SWNT (yellow) in the leaf epidermis shows localization on the plasma membrane stained with membrane-selective FM4-64 dye (red). **b,** Cy3-labelled G-SWNT (yellow) is colocalized with the FM4-64-stained plasma membrane (red) as well as within the chloroplasts (magenta) in the mesophyll cell of spinach leaf. For **a** and **b**, *n* = 5 independent biological experiments were repeated with similar results.

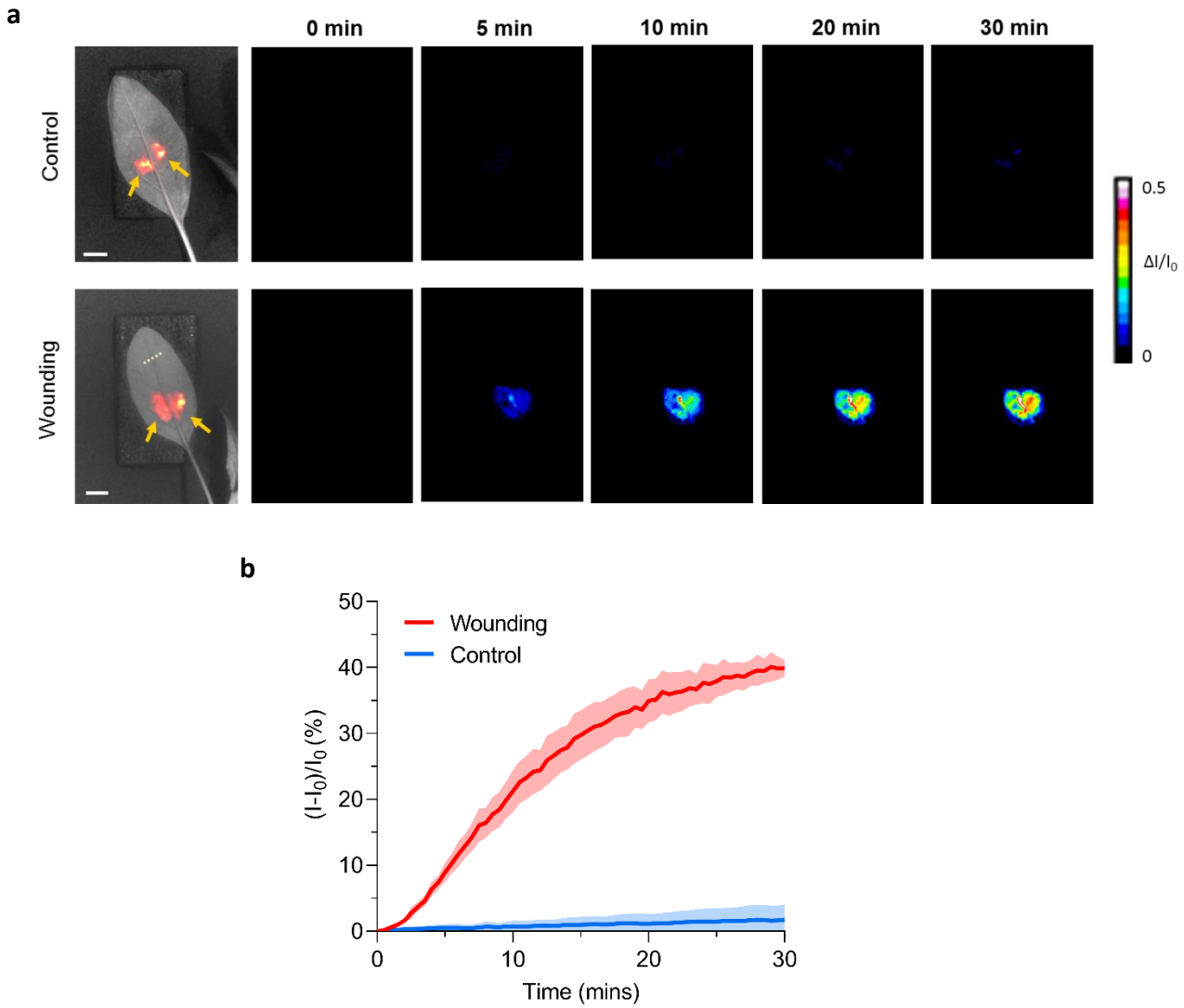


**Supplementary Figure 6. Detection of wound-induced ROS accumulation with $H_2$DCFDA as a comparison to the nanosensor tool. a**, False-colored time-lapse images showing the change in fluorescence intensity of $H_2$DCFDA (yellow arrows) upon plant wounding (dashed line) in spinach. $n$ = 3 independent biological experiments were repeated with similar results obtained. Scale bars, 5 mm. **b,** Time profile of $H_2$DCFDA fluorescence intensity change after wounding shows irreversible increase compared to non-treated control plants. Shaded regions represent s.e.m. from $n$ = 3 biologically independent plants.

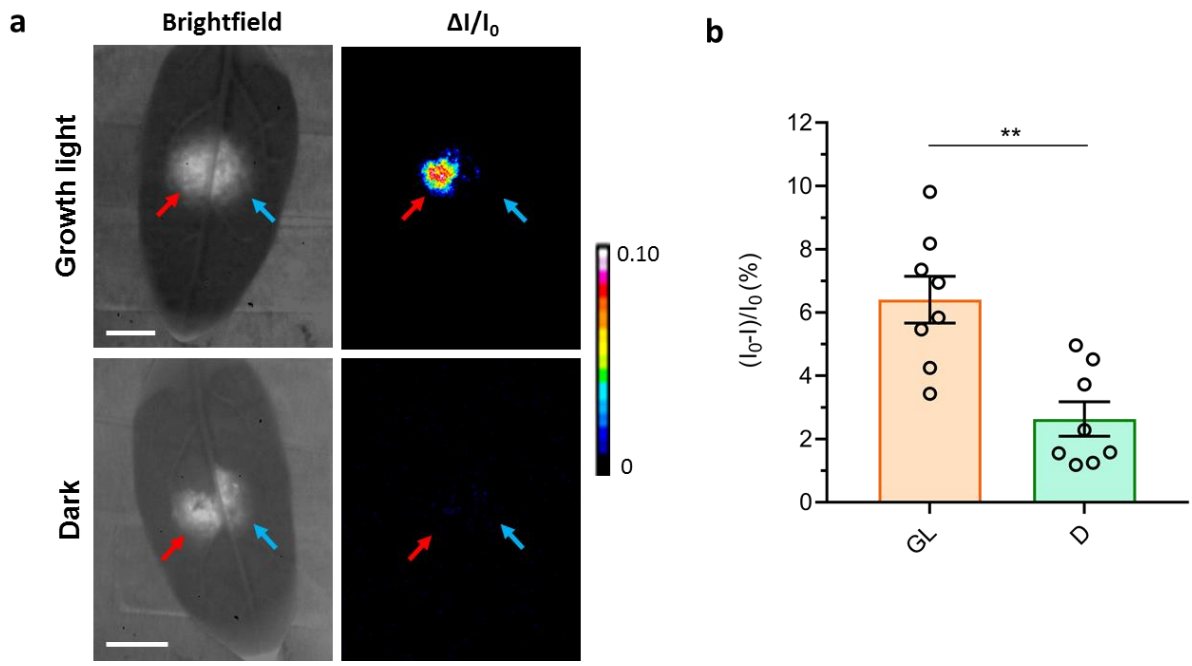


**Supplementary Figure 7. Sensitivity of G-SWNT and A-SWNT to detect basal $H_2O_2$ level in planta due to natural light. a,** False-colored images showing the change in G-SWNT (red arrow) and A-SWNT (blue arrow) fluorescence intensity before and after the plants were subjected to growth light (top) or dark condition (bottom) for 4 hours. Scale bars, 5 mm. *n* = 8 independent biological experiments were repeated with similar results obtained. **b,** Average change in G-SWNT fluorescence intensity before and after the plants were kept in growth light (GL) and dark (D) conditions. Data are mean ± s.e.m., with *n* = 8 biologically independent samples. Two-tailed unpaired *t*-test, **P = 0.0012.

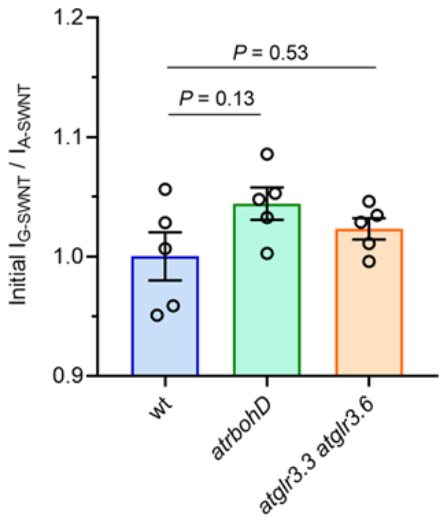


**Supplementary Figure 8. Nanosensors probe basal $H_2O_2$ level in *Arabidopsis thaliana* mutants.** Comparison of the initial fluorescence intensity of G-SWNT to A-SWNT for wild-type, *rbohD* mutant and *glr3.3 glr3.6* mutant of *Arabidopsis thaliana*. One-way ANOVA with the Newman-Keuls post-hoc test. Data are mean ± s.e.m., with $n = 5$ biologically independent samples.

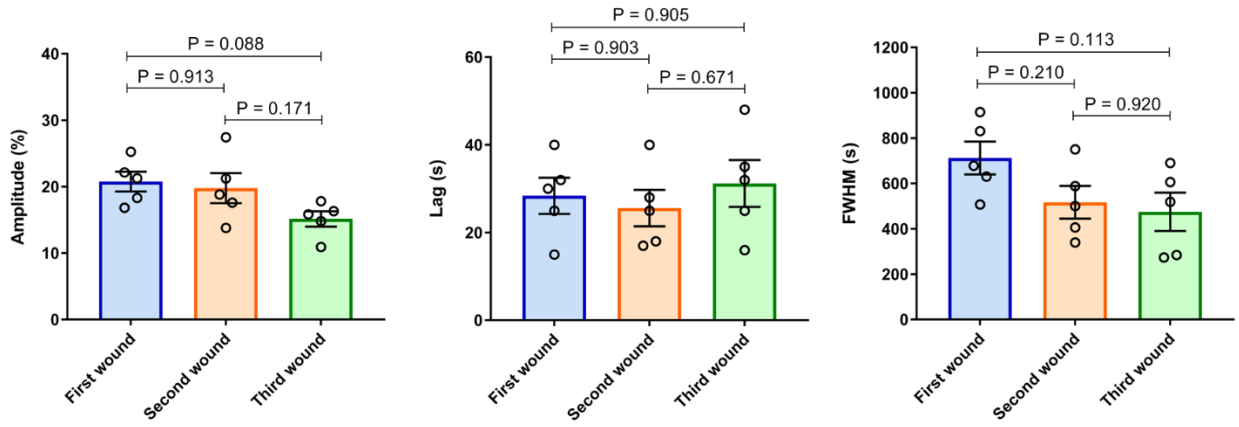


**Supplementary Figure 9. Characterization of sensor response due to repeated wounding in planta.** Wounding response was characterized in terms of amplitude, lag and full-width-of-half-maximum (FWHM) of the ratiometric platform output. No statistically significant difference in the wave properties was observed between wounding. One-way ANOVA with the Newman-Keuls post-hoc test. Data are mean ± s.e.m., with $n = 5$ biologically independent samples.

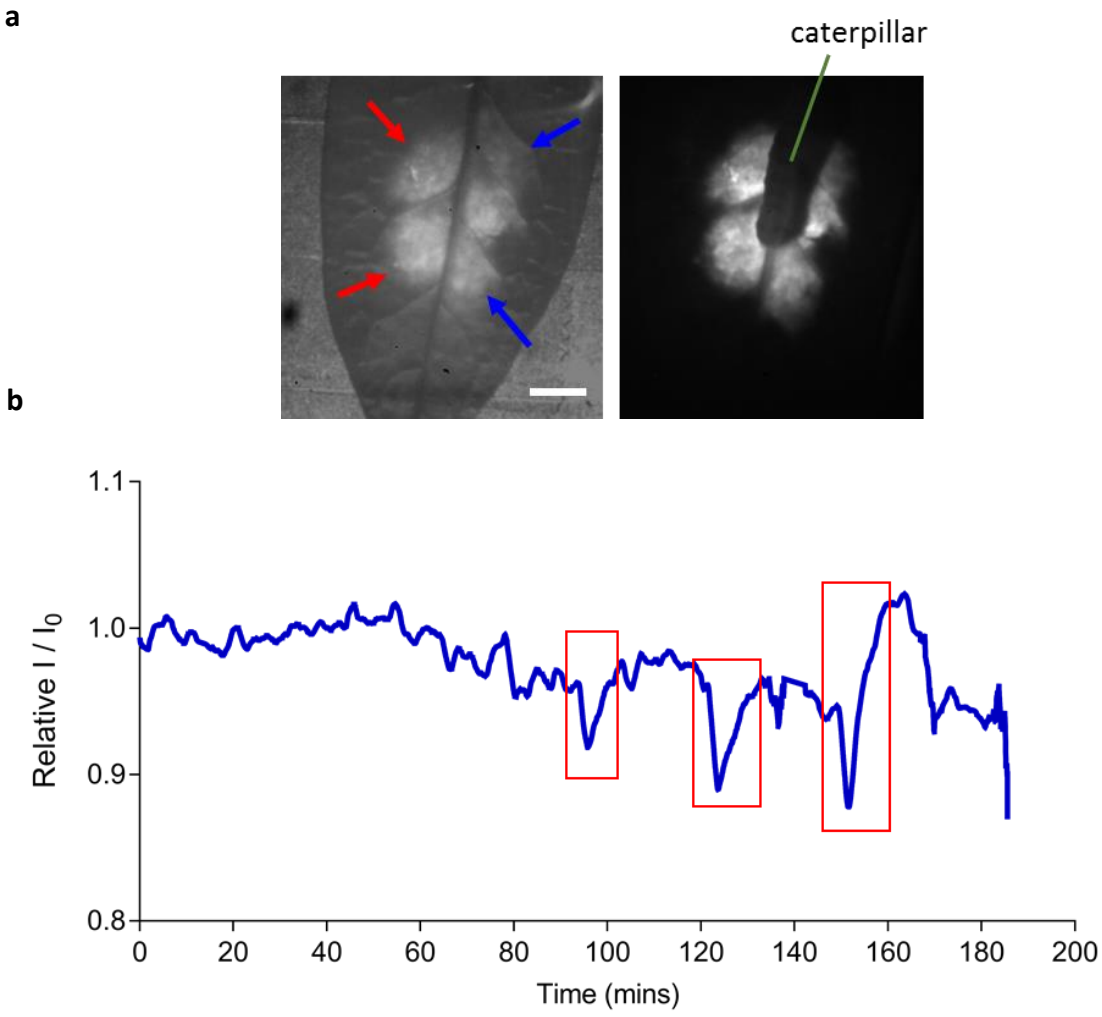


**Supplementary Figure 10. Application of SWNT sensors to detect $H_2O_2$ induced by insect feeding. a,** (Left) Brightfield image of an intact spinach plant leaf infiltrated with G-SWNT and A-SWNT. Red and blue arrows indicate G-SWNT and A-SWNT respectively. Scale bar, 5 mm. (Right) Image of caterpillar on the leaf lamina. **b,** 3-hour time profile of the G-SWNT/A-SWNT ratio to monitor $H_2O_2$ produced from mechanical wounding due to insect feeding. Red boxes indicate the characteristic wound-induced $H_2O_2$ wave. $n$ = 3 independent biological experiments were repeated with similar results obtained.

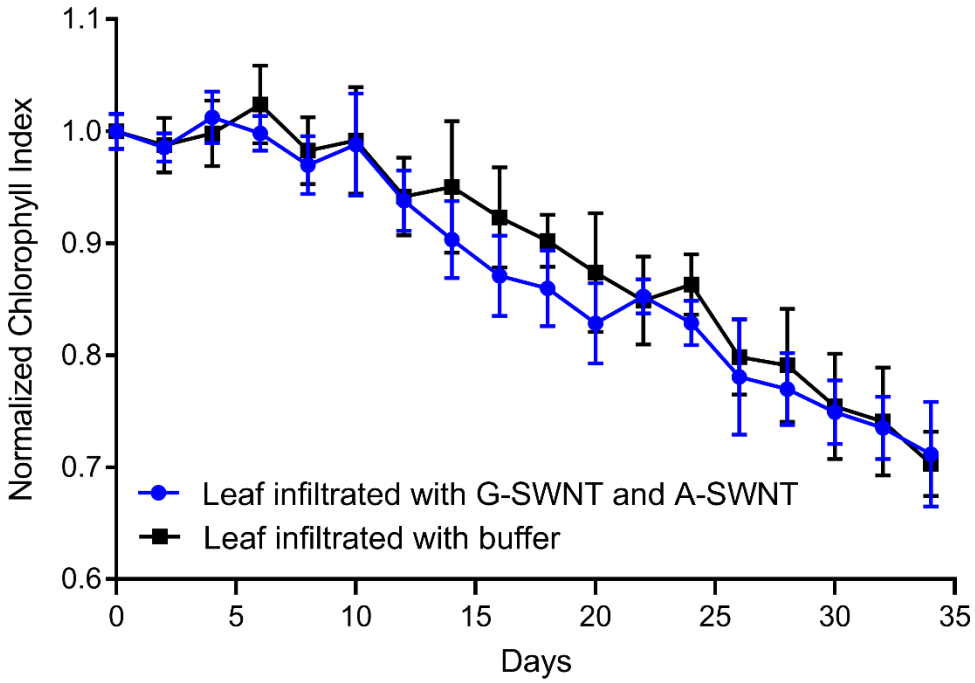


**Supplementary Figure 11. Time profile of leaf chlorophyll content after nanosensor infiltration.** There was no significant difference in the leaf lifespan between leaf infiltrated with G-SWNT and A-SWNT, and leaf infiltrated with MES-$MgCl_2$ buffer over a period of 5 weeks. Data are mean ± s.e.m., with $n = 5$ biologically independent samples.

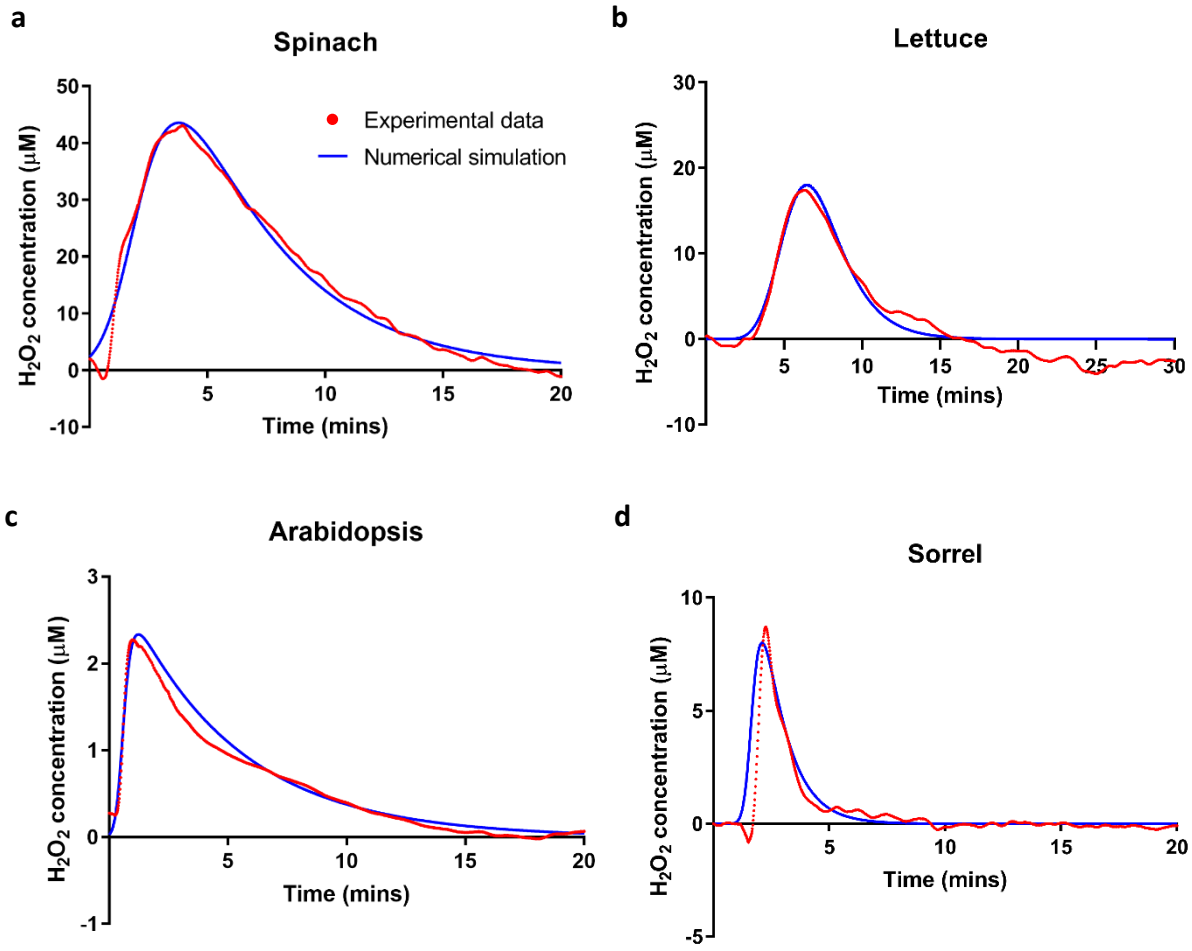


**Supplementary Figure 12. Fitting of wound-induced $H_2O_2$ temporal profile with the numerical solution of the autocatalytic propagation model.** Fitting of experimental data (red) of **a**, spinach, **b**, lettuce, **c**, *Arabidopsis thaliana*, and **d**, sorrel with model predictions (blue).

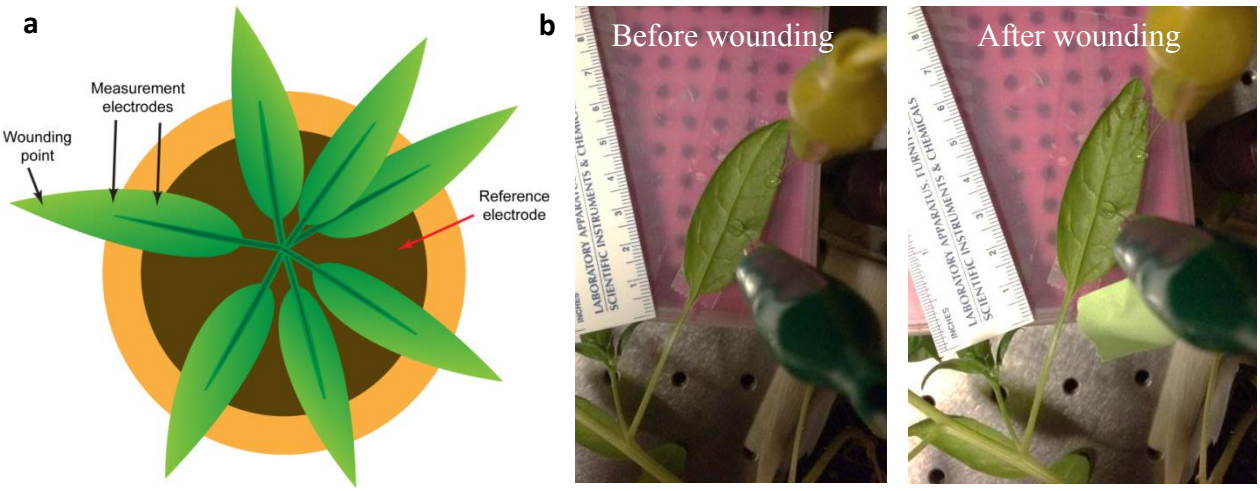


**Supplementary Figure 13. Electrical wave measurement in plants.** Schematic configuration, **a**, and photographs, **b**, of the electrodes contacting the leaf lamina for electrical monitoring of the wounding response.

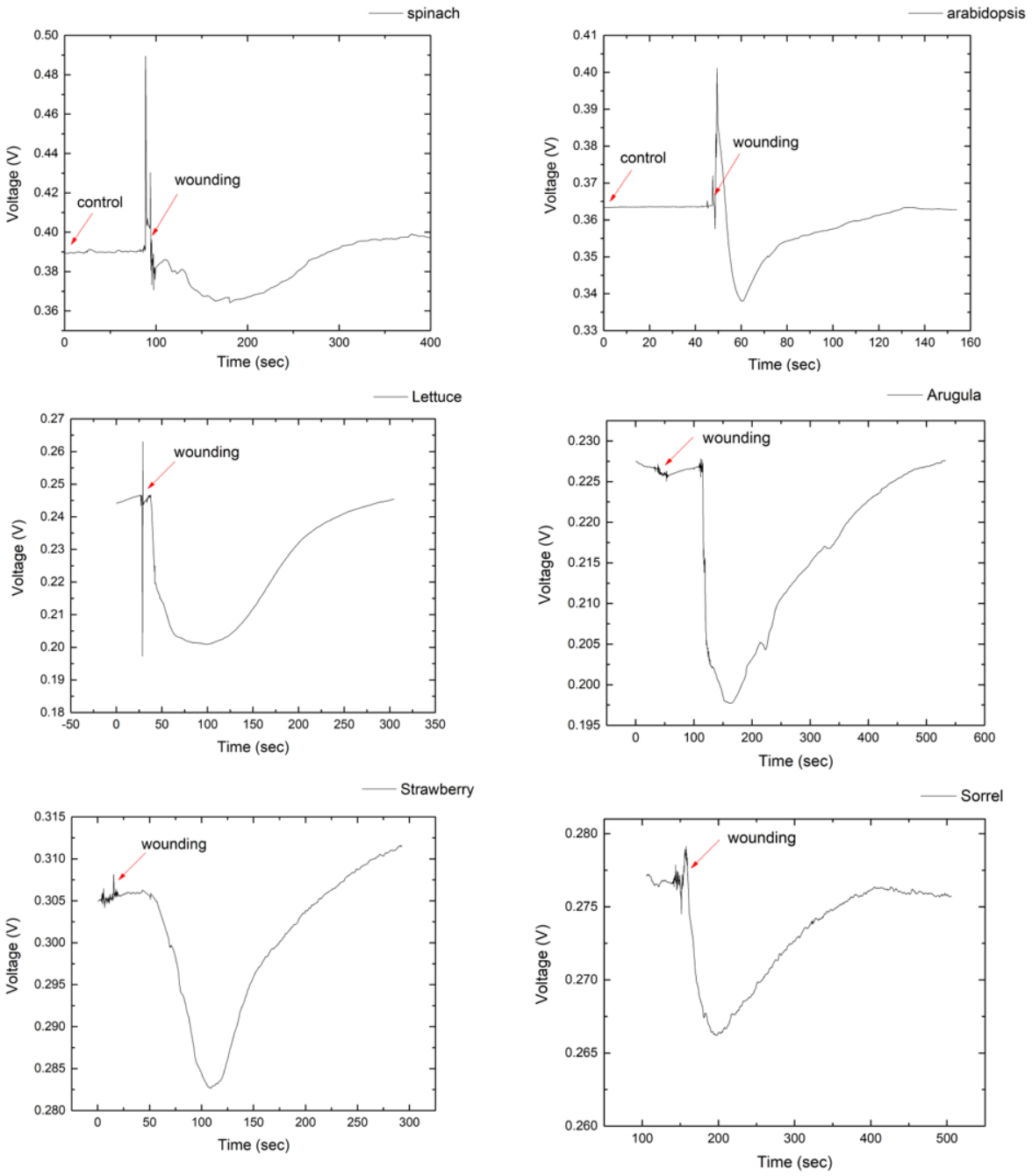


**Supplementary Figure 14. Representative electrical responses for the studied species.** The electrical responses in six plant species were recorded using the setup illustrated in Supplementary Figure 13.

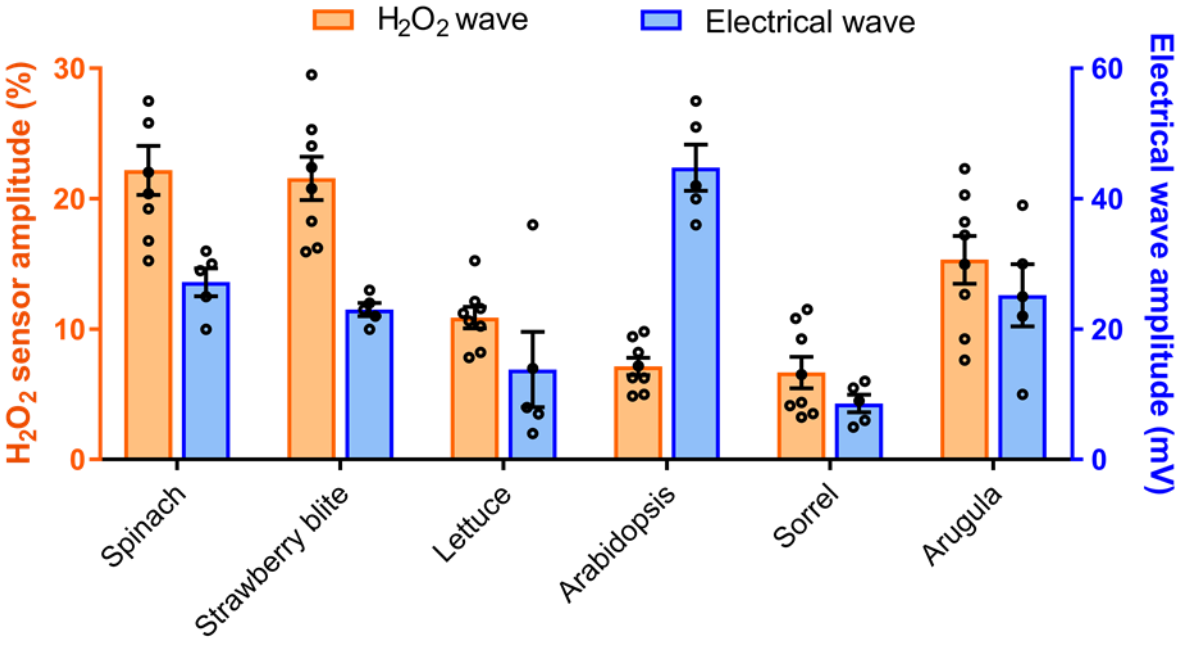


**Supplementary Figure 15. Comparison of $H_2O_2$ and electrical wave characteristics.** Amplitude profile of $H_2O_2$ and electric signal due to wounding in different plant species. Data are mean ± s.e.m. $n = 8$ and $n = 5$ biologically independent samples for $H_2O_2$ wave and electrical wave amplitude respectively.

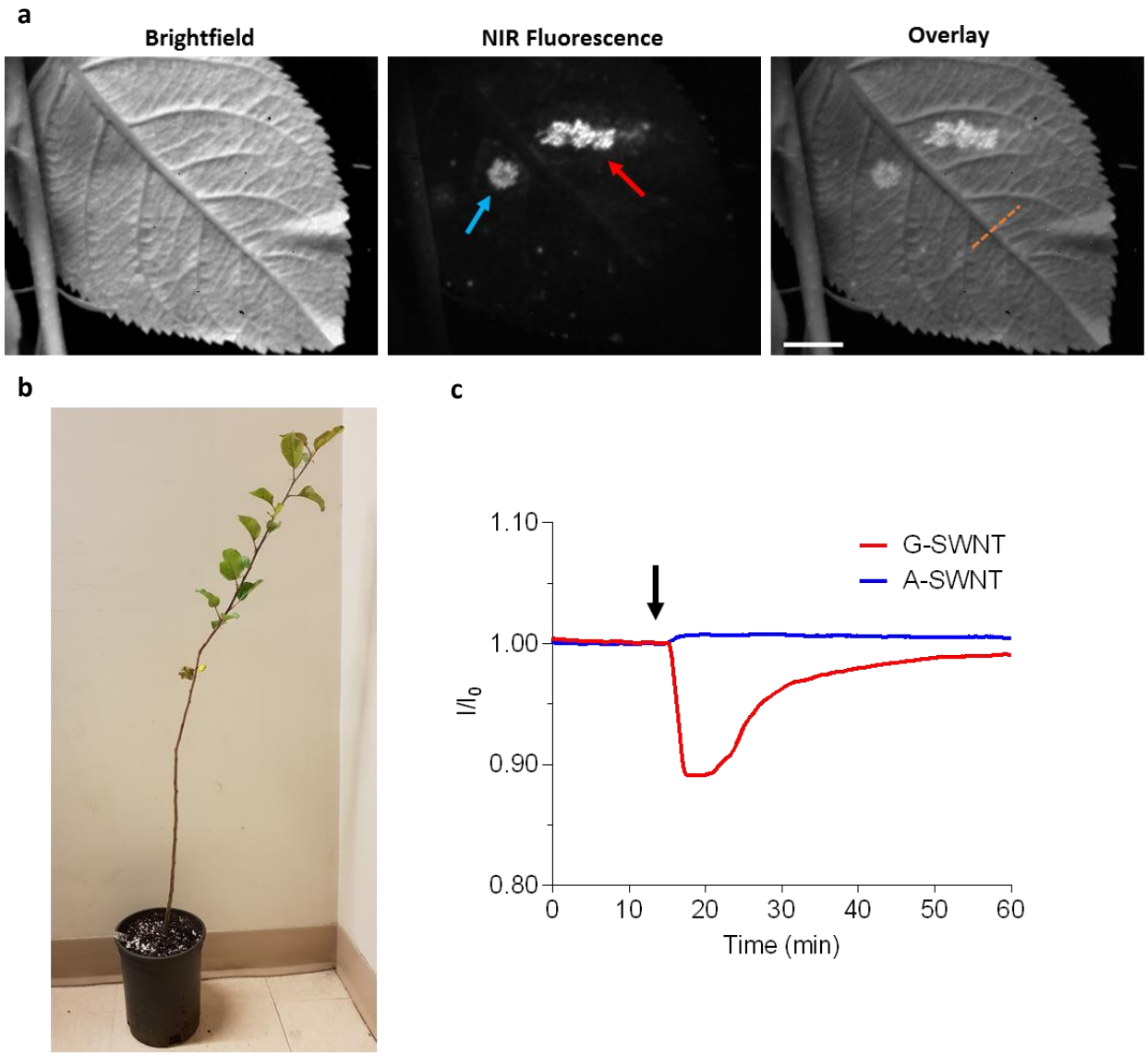


**Supplementary Figure 16. Nanosensor application to monitor wounding response from 2-year-old Fuji apple tree. a,** Images of a Fuji apple tree leaf infiltrated with G-SWNT and A-SWNT. Red and blue arrows indicate G-SWNT and A-SWNT respectively. Dashed line represents the location of wounding. Scale bar, 1 cm. **b,** Photograph of the 2-year-old Fuji apple tree. Scale bar, 30 cm. **c**, Time-profile of G-SWNT and A-SWNT in response to wounding on the Fuji apple tree leaf. Black arrow indicates the time point of wounding. $n$ = 3 independent biological experiments were repeated with similar results obtained.

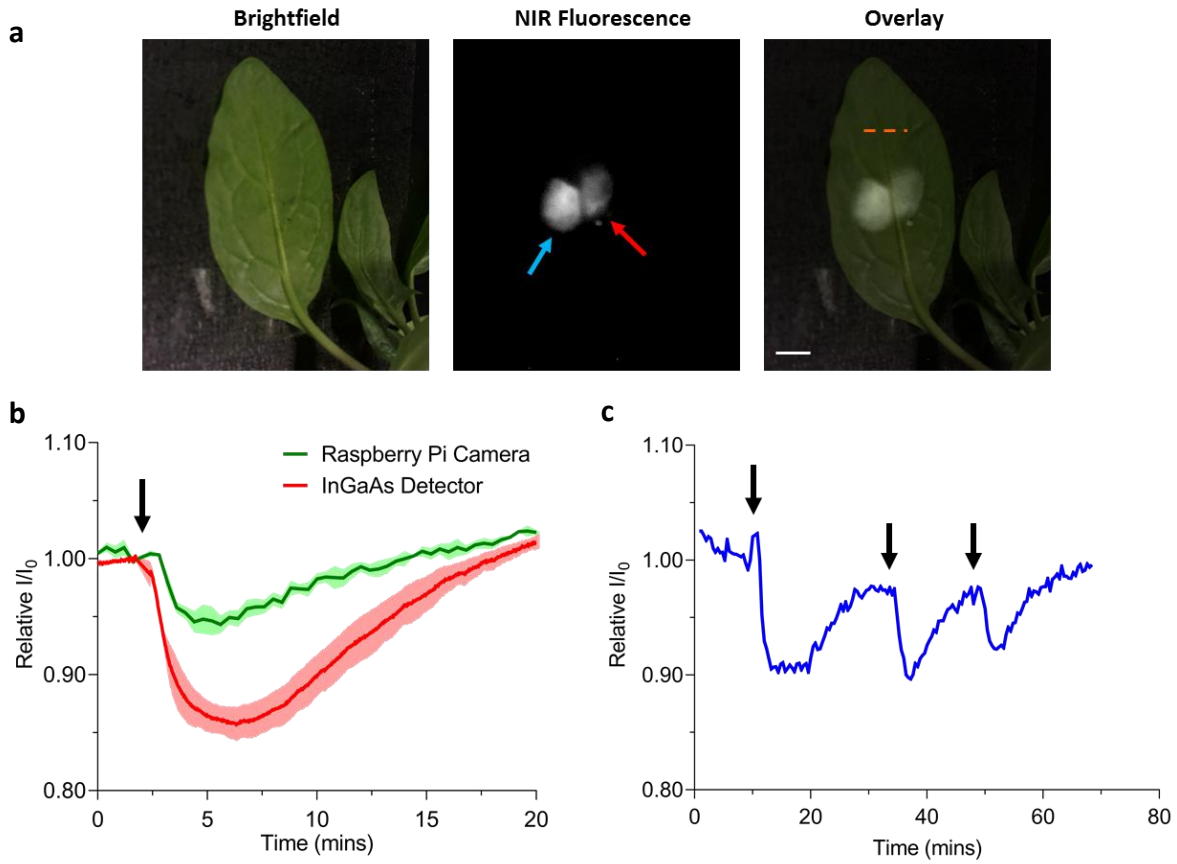


**Supplementary Figure 17. Standoff detection of wound-induced $H_2O_2$ signal with Raspberry Pi platform. a**, Brightfield and sensor images of a spinach plant leaf infiltrated with G-SWNT and A-SWNT as obtained with a Raspberry Pi CCD detector (infrared filters removed). Blue and red arrows represent A-SWNT and G-SWNT respectively. Dashed line represents the location of wounding. Scale bar, 5 mm. **b**, Simultaneous detection of wound-induced $H_2O_2$ signal with Raspberry Pi CCD detector and InGaAs detector. Shared regions represent s.e.m. from $n$ = 3 biologically independent plants. **c,** Repeated wounding resulted in multiple $H_2O_2$ signal propagation as detected by a Raspberry Pi CCD detector. Black arrows represent the time point of wounding. $n$ = 3 independent biological experiments were repeated with similar results obtained.

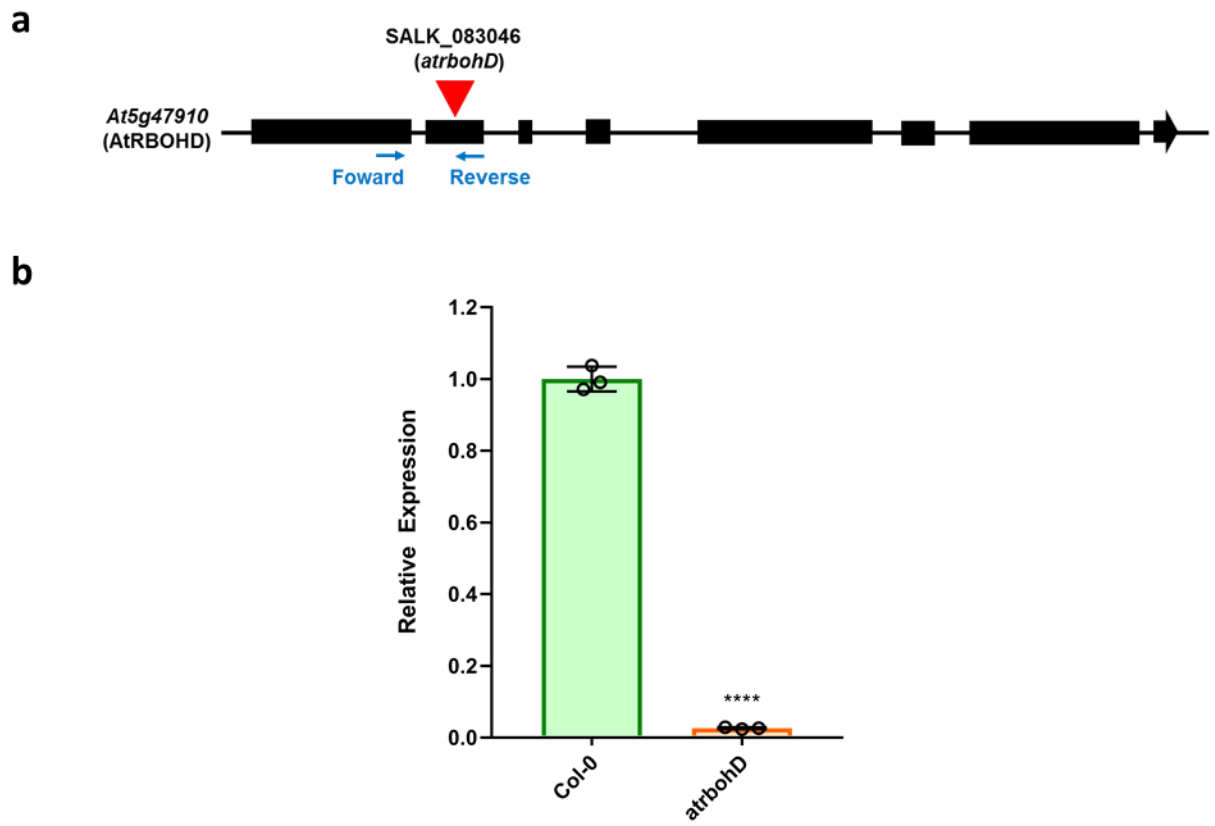


**Supplementary Figure 18. Expression analyses of *atrbohD* mutant. a,** Schematic diagram of genomic structure of *AtRBOHD*. T-DNA insertion location (red triangle) of *atrbohD* mutant (salk_083046) and qPCR primers (blue arrow) were described in the diagram. **b,** *AtRBOHD* transcription level in Col-0 and *atrbohD* mutant. Transcript levels were normalized to *ACT2* expression levels. Data are mean ± s.d. from $n = 3$ independent seedling pools. Two-tailed unpaired *t*-test, ****P < 0.0001.

| **Plant species** | **Treatment** | $\alpha$ |
|---|---|---|
| Spinach *(Spinacia oleracea)* | None | 0.19 |
| | DPI | 0.36 |
| | $LaCl_3$ | 0.25 |
| | Catalase | 0.39 |
| | Caffeic acid | 0.33 |
| Strawberry blite *(Blitum capitatum)* | None | 0.17 |
| Lettuce *(Lactuca sativa)* | None | 0.75 |
| *Arabidopsis thaliana* | None | 0.04 |
| Sorrel *(Rumex acetosa)* | None | 0.08 |
| Arugula *(Eruca sativa)* | None | 0.54 |

**Supplementary Table 1.** Fitted value of $\alpha$ across species based on wound-induced $H_2O_2$ response.

**Video Legends**

**Supplementary Video 1. False-colored video of nanosensors' response towards wounding in a spinach leaf.** G-SWNT and A-SWNT were infiltrated on the left and right side of the midrib respectively. This corresponds to the same leaf as that depicted in Figure 2b. P and W denote pre-wounding and post-wounding frames respectively, with the white frames representing the wounding event. Time is in mm:ss format. Scale bar, 5 mm.

**Supplementary Video 2. Real-time response of nanosensors upon insect feeding on a spinach leaf.** G-SWNT and A-SWNT were infiltrated on the left and right side of the midrib respectively. This corresponds to the same leaf as that depicted in Supplementary Figure 10. W1, W2 and W3 denote the first, second and third instance of nanosensors' response recorded upon insect feeding. Time is in mm:ss format. Scale bar, 5 mm.

**Supplementary Video 3. Spatiotemporal profile of G-SWNT sensor response due to wounding**. This corresponds to the same leaf as that depicted in Figure 4d. P and W denote pre-wounding and post-wounding frames respectively, with the white frames representing the wounding event. Time is in mm:ss format. Scale bar, 5 mm.